Taylor & Francis
Taylor & Francis Group

Vehicle System Dynamics
International Journal of Vehicle Mechanics and Mobility

ISSN: 0042-3114 (Print) 1744-5159 (Online) Journal homepage: http://www.tandfonline.com/loi/nvsd20

Full drive-by-wire dynamic control for four-wheel-steer all-wheel-drive vehicles

Farbod Fahimi

To cite this article: Farbod Fahimi (2013) Full drive-by-wire dynamic control for four-wheel-steer all-wheel-drive vehicles, Vehicle System Dynamics, 51:3, 360-376, DOI: 10.1080/00423114.2012.743668

To link to this article: http://dx.doi.org/10.1080/00423114.2012.743668

Published online: 21 Nov 2012.

Vehicle System Dynamics, 2013
Vol. 51, No. 3, 360–376, http://dx.doi.org/10.1080/00423114.2012.743668

Full drive-by-wire dynamic control for four-wheel-steer all-wheel-drive vehicles

Farbod Fahimi*

UAHuntsville, MAE, 5000 Technology Drive, Huntsville, AL 35899, USA

(*Received 19 March 2012; final version received 18 October 2012*)

Most of the controllers introduced for four-wheel-steer (4WS) vehicles are derived with the assumption that the longitudinal speed of the vehicle is constant. However, in real applications, the longitudinal speed varies, and the longitudinal, lateral, and yaw dynamics are coupled. In this paper, the longitudinal dynamics of the vehicle as well as its lateral and yaw motions are controlled simultaneously. This way, the effect of driving/braking forces of the tires on the lateral and yaw motions of the vehicle are automatically included in the control laws. To address the dynamic parameter uncertainty of the vehicle, a chatter-free variable structure controller is introduced. Elimination of chatter is achieved by introducing a dynamically adaptive boundary layer thickness. It is shown via simulations that the proposed control approach performs more robustly than the controllers developed based on dynamic models, in which longitudinal speed is assumed to be constant, and only lateral speed and yaw rate are used as system states. Furthermore, this approach supports all-wheel-drive vehicles. Front-wheel-drive or rear-wheel-drive vehicles are also supported as special cases of an all-wheel-drive vehicle.

Keywords: drive-by-wire; four-wheel-steer; all-wheel-drive; robust control; stability control; bicycle model

1. Introduction

During the last two decades, researchers have worked on improving the dynamic stability of vehicles. One of the several approaches for achieving that improvement is to introduce rear steering along with the conventional front steering. A four-wheel-steer (4WS) vehicle is capable of better handling due to the availability of an extra control input, the rear steering angle.

Researchers have shown that the stability of a 4WS vehicle can be significantly improved by closed-loop control. Table 1 summarises the research on closed-loop control of 4WS vehicles. It can be seen that several approaches to the closed-loop control problem exist.

Different types of control input have been used. Many researchers have used only the rear steer angle as an stability aid [3,14–16,19,20,22,23]. In this approach, the longitudinal speed of the vehicle is assumed to be constant, and it is assumed that a driver decides the front steering angle based on his/her desired manoeuvre. In this approach, researchers

*Corresponding author. Email: farbod.fahimi@uah.edu, fahimi@eng.uah.edu

Table 1. Summary of related research.

	Inputs				Outputs					Control method								
Reference	Front steer angle	Rear steer angle	Lateral force	Steer moment	Braking force	Sideslip angle	Yaw rate	Axle positions	Lateral speed	μ-Synthesis	Sliding mode	Fuzzy	PID	Decoupled	Internal model	H_∞	Time delay	Linear programming
[1]	x	x	–	–	–	x	x	–	–	x	–	–	–	–	–	–	–	–
[2]	–	–	x	x	–	x	x	–	–	–	x	–	–	–	–	–	–	–
[3]	–	x	–	x	–	x	x	–	–	–	–	x	–	–	–	–	–	–
[4]	x	x	–	–	–	x	x	–	–	x	–	–	–	–	–	–	–	–
[5]	–	x	–	–	–	–	x	–	–	–	–	–	x	–	–	–	–	–
[6]	x	x	–	–	–	–	–	x	–	–	x	–	–	–	–	–	–	–
[7]	x	x	–	–	–	–	x	–	x	–	–	–	–	x	–	–	–	–
[8]	x	x	–	–	–	–	x	–	x	–	x	x	–	–	–	–	–	–
[9]	x	x	–	–	–	x	x	–	–	–	–	–	–	–	x	–	–	–
[10]	x	x	–	–	–	x	x	–	–	–	–	x	–	–	–	–	–	–
[11]	x	x	–	–	–	x	x	–	–	x	–	–	–	–	–	–	–	–
[12]	x	x	–	–	–	–	x	–	x	–	–	–	x	x	–	–	–	–
[13]	x	x	–	–	–	–	x	–	x	–	–	–	–	–	–	x	–	–
[14]	–	x	–	–	–	x	x	–	–	–	–	x	–	–	–	–	–	–
[15]	–	x	–	–	–	–	x	–	–	–	–	–	x	–	–	–	–	–
[16]	–	x	–	–	–	–	x	–	–	–	–	–	–	–	–	–	–	–
[17]	x	x	–	–	x	–	x	–	–	–	–	–	–	–	–	–	–	–
[18]	x	x	–	–	–	–	x	–	–	–	–	–	x	x	–	–	–	–
[19]	–	x	–	–	–	x	–	–	–	–	–	x	–	–	–	–	–	–
[20]	–	x	–	–	–	x	–	–	–	–	–	–	x	–	–	–	–	–
[21]	x	x	–	–	x	–	x	–	–	–	–	–	–	–	–	x	–	–
[22]	–	x	–	–	–	–	x	–	–	–	–	–	–	–	–	–	x	–
[23]	–	x	–	–	x	–	x	–	–	–	–	–	–	–	–	–	–	x

Note: PID: proportional–integral–derivative. An ‘x’ in a column indicates that the corresponding feature has been used in the cited reference in the respective row.

have used either the sideslip angle or the yaw rate, or their combination, as a measure of stability (Table 1).

Other researchers have defined both the front and rear steer angles as control inputs (Table 1). This approach is more suitable for drive-by-wire implementation. In this approach, the longitudinal speed of the vehicle is assumed to be constant. Normally, a desired yaw rate and a sideslip angle are generated by processing the vehicle speed and the steering wheel position controlled by a driver. The controller, then, tracks the yaw rate and the sideslip angle. In some cases, the lateral speed replaces the sideslip angle [7,8,12,13]. In rare cases, the steer moment or braking forces are used as control inputs [2,3,17,21,23].

Mostly linear control methods along with linearised models are reported. These control methods include proportional–integral–derivative [5,15,20], decoupled [7,12,18], H_∞ [13,21], time delay [22], and linear programming [23]. Non-conventional and nonlinear robust control methods are also used; however, the vehicle dynamic models for control design are still linearised. Fuzzy control [3,10,14,19], sliding mode [2,6,8], μ-synthesis [1,4,11], and hybrid fuzzy-sliding mode control [12] are reported in the literature.

In summary, as can be concluded from the literature survey presented in this section, most of the controllers introduced for 4WS vehicles are derived based on the assumption that the longitudinal speed of the vehicle is kept constant. However, in most practical cases, the speed of the vehicle is increased or decreased while the vehicle moves on a curve. While the speed is increasing or decreasing, the driving/braking forces underneath the tires change. Since all the tires of a 4WS vehicle are steered, these driving/braking forces have components in the lateral direction. These components affect the yaw and lateral motion of the vehicle. Neglecting the effect of these forces lead to inferior control performance on sharper turns.

In this paper, a different approach is proposed. The longitudinal dynamics of the vehicle as well as its lateral and yaw motions are controlled simultaneously. This way, the effect of driving/braking forces of the tires on the lateral and yaw motions of the vehicle are automatically included in the control laws. This is done by considering a 3-degree-of-freedom (3DOF) dynamic model, including the longitudinal speed, the lateral speed, and the yaw rate, for controller derivations. In addition, to address the dynamic parameter uncertainty of the vehicle, a chatter-free variable structure controller is introduced. Chattering is avoided by introducing a boundary layer with dynamically variable thickness. As a result, the proposed control approach performs more robustly than the controllers developed based on a 2-degree-of-freedom (2DOF) conventional dynamic model, in which the longitudinal speed is assumed to be constant, and only the lateral speed and the yaw rate are used. Furthermore, this approach supports all-wheel-drive vehicles. Front-wheel-drive or rear-wheel-drive vehicles are also supported as special cases of an all-wheel-drive vehicle.

2. Dynamic model

2.1. *6DOF nonlinear vehicle model with the Pacejka tire model*

A general 6-degree-of-freedom (6DOF) model is considered to closely represent the nonlinear dynamics of the vehicle (Figure 1(a)). The Pacejka tire model is used for simulating the lateral tire forces. This model is used for verifying the performance of different controllers in simulations. The nonlinear dynamic model of the vehicle is described as follows:

$$\sum_{i=1}^{4} \mathbf{F}_i^{\mathrm{B}} + m\mathbf{g}^{\mathrm{B}} = m(\dot{\mathbf{V}}_G^{\mathrm{B}} + \boldsymbol{\omega}^{\mathrm{B}} \times \mathbf{V}_G^{\mathrm{B}}) \quad \text{and} \quad \sum_{i=1}^{4} \mathbf{d}_i^{\mathrm{B}} \times \mathbf{F}_i^{\mathrm{B}} = \mathbf{I}_G^{\mathrm{B}} \dot{\boldsymbol{\omega}}^{\mathrm{B}} + \boldsymbol{\omega}^{\mathrm{B}} \times \mathbf{I}_G^{\mathrm{B}} \boldsymbol{\omega}^{\mathrm{B}}, \qquad (1)$$

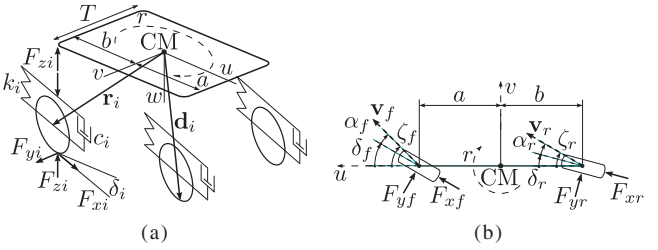

Figure 1. (a) 6DOF vehicle model; (b) 3DOF vehicle model.

where $\mathbf{d}_i^{\mathrm{B}}$ points from the origin of the body coordinate axes to the contact point of the wheel i and the ground, and

$$\mathbf{V}_G^{\mathrm{B}} = [u, v, w], \quad \boldsymbol{\omega}^{\mathrm{B}} = [p, q, r], \quad \mathbf{F}_i^{\mathrm{B}} = \begin{bmatrix} F_{xi}\cos\delta_i - F_{yi}\sin\delta_i - C_{\mathrm{D}}A_{\mathrm{D}}u^2 \\ F_{xi}\sin\delta_i + F_{yi}\cos\delta_i \\ -F_{zi} \end{bmatrix}^{\mathrm{T}}. \tag{2}$$

$\mathbf{I}_G^{\mathrm{B}}$ is the moment of inertia of the vehicle body and $\mathbf{g}^{\mathrm{B}}$ is the acceleration of gravity. The superscript 'B' indicates that all components are in terms of the vehicle body coordinates. F_{zi} is the normal force exerted on the vehicle chassis by the suspension of wheel i. The suspension force is calculated using the deflection of the suspension spring z_i and its rate of change:

$$F_{zi} = k_i(z_i + z_{i0}) + c_i\dot{z}_i, \tag{3}$$

where z_{i0} is the static deflection in the suspension, with equivalent stiffness k_i and damping c_i, under the vehicle's weight ($\sum_{i=1}^{4} k_i z_{i0} = mg$) at static equilibrium on a flat horizontal surface, where body roll and pitch angles are assumed to be zero. At any given time, on a flat horizontal road, the spring deflections are calculated using the body roll and pitch angles.

The angle ξ_i that the wheel's centre velocity vector makes with the vehicle's longitudinal axis is determined by

$$\xi_i = \cos^{-1}\left[\frac{\mathbf{V}_G^{\mathrm{B}} + \boldsymbol{\omega}^{\mathrm{B}} \times \mathbf{r}_i^{\mathrm{B}}}{|\mathbf{V}_G^{\mathrm{B}} + \boldsymbol{\omega}^{\mathrm{B}} \times \mathbf{r}_i^{\mathrm{B}}|} \cdot \hat{\mathbf{i}}^{\mathrm{B}}\right], \tag{4}$$

where $\mathbf{r}_i^{\mathrm{B}}$ points from the origin of the body coordinate to the centre of the wheel i. The slip angle is defined as $\alpha_i = \xi_i - \delta_i$. The lateral force of each tire is calculated by using the tire normal force from Equation (3) and the tire slip angle with the Pacejka tire model:

$$\begin{aligned} &C = 1.30, \quad D = a_1F_{zi}^2 + a_2F_{zi}, \quad BCD = a_3\sin(a_4\tan^{-1}(a_5F_{zi})), \\ &B = \frac{BCD}{CD}, \quad E = a_6F_{zi}^2 + a_7F_{zi} + a_8, \quad \phi = (1-E)\alpha_i + \frac{E}{B}\tan^{-1}(B\alpha_i), \\ &F_{yi} = A_kD\sin(C\tan^{-1}(B\phi)), \end{aligned} \tag{5}$$

where a_1–a_8 are tire parameters, F_{zi} and α_i are in kN and degrees, respectively, and A_k is a magnification factor (where subscript k is replaced by f for the front wheels and by r for the rear wheels).

2.2. *Proposed 3DOF simplified nonlinear model*

A general 3DOF model is considered to represent the nonlinear dynamics of the vehicle closely (Figure 1(b)) for the purpose of the controller design:

$$\begin{aligned} m(\dot{u} - rv) &= F_{xf}\cos(\delta_f) - F_{yf}\sin(\delta_f) + F_{xr}\cos(\delta_r) - F_{yr}\sin(\delta_r) - C_D A_D u^2, \\ m(\dot{v} + ru) &= F_{xf}\sin(\delta_f) + F_{yf}\cos(\delta_f) + F_{xr}\sin(\delta_r) + F_{yr}\cos(\delta_r), \\ I_z\dot{r} &= aF_{xf}\sin(\delta_f) + aF_{yf}\cos(\delta_f) - bF_{xr}\sin(\delta_r) - bF_{yr}\cos(\delta_r), \end{aligned} \tag{6}$$

where

$$F_{yf} = -C_{\alpha f}(\xi_f - \delta_f), \quad F_{yr} = -C_{\alpha r}(\xi_r - \delta_r), \tag{7}$$

where $C_{\alpha f}$ and $C_{\alpha r}$ are the slope of lines fitted to the linear portion of the lateral force versus slip angle curves ($-5^\circ < \alpha < 5^\circ$) derived from the Pacejka model (Equation 5) for nominal vertical tire force ($\frac{1}{4}$ of vehicle's weight).

$$\xi_f = \tan^{-1}\left(\frac{v + ra}{u}\right), \quad \xi_r = \tan^{-1}\left(\frac{v - rb}{u}\right), \quad u \neq 0. \tag{8}$$

It is assumed that γ portion of the total driving force F_x is exerted on the front axle, and the remaining driving force is exerted on the rear axle, where $0 \leq \gamma \leq 1$. So,

$$F_{xf} = \gamma F_x, \quad F_{xr} = (1 - \gamma)F_x. \tag{9}$$

For a front-wheel-drive vehicle, $\gamma = 1$, and for a rear-wheel-drive vehicle, $\gamma = 0$.

The 3DOF nonlinear bicycle model of the vehicle is simplified in this subsection. The simplifications aim at a model that can be used for designing a robust controller, which simultaneously controls all 3DOFs of the bicycle model. The simplified model is found by assuming that effective steer angles ($\xi_i, i = r, f$) are small, so that $\tan(\xi_i) \approx \xi_i$. Furthermore, it is assumed that steering angles ($\delta_i, i = r, f$) are small, so that $\cos(\delta_i) \approx 1$, $\sin(\delta_i) \approx \delta_i$, and $\delta_i \sin(\delta_i) \neq 0$. Using these assumptions, and substituting Equations (7) and (8) into Equation (6), one arrives at the following matrix equation:

$$\mathbf{M}[\dot{u}\ \dot{v}\ \dot{r}]^T + \mathbf{A}_1[u\ v\ r]^T + \mathbf{B}_1[F_x\ \delta_f\ \delta_r]^T + \mathbf{W}_1 = \mathbf{0}, \tag{10}$$

where

$$\mathbf{M} = \begin{bmatrix} m & 0 & 0 \\ 0 & m & 0 \\ 0 & 0 & I_z \end{bmatrix}, \quad \mathbf{A}_1 = \begin{bmatrix} C_D A_D u & 0 & 0 \\ 0 & \dfrac{C_{\alpha f} + C_{\alpha r}}{u} & mu + \dfrac{C_{\alpha f}a - C_{\alpha r}b}{u} \\ 0 & \dfrac{C_{\alpha f}a - C_{\alpha r}b}{u} & \dfrac{C_{\alpha f}a^2 + C_{\alpha r}b^2}{u} \end{bmatrix}, \tag{11}$$

$$\mathbf{B}_1 = \begin{bmatrix} -1 & C_{\alpha f}\left(\dfrac{v + ar}{u}\right) & C_{\alpha r}\left(\dfrac{v - br}{u}\right) \\ 0 & -C_{\alpha f} & -C_{\alpha r} \\ 0 & -aC_{\alpha f} & bC_{\alpha r} \end{bmatrix}, \quad \mathbf{W}_1 = \begin{bmatrix} C_{\alpha f}\delta_f\sin(\delta_f) + C_{\alpha r}\delta_r\sin(\delta_r) \\ -\gamma F_x\delta_f - (1 - \gamma)F_x\delta_r \\ -a\gamma F_x\delta_f + b(1 - \gamma)F_x\delta_r \end{bmatrix}. \tag{12}$$

Note that the simplified model represented by Equation (10) still includes nonlinear terms in the vector $\mathbf{W}$. These nonlinear terms play an important role in designing a robust controller.

The simplified model in Equation (10) is used as the plant model. The input vector to the plant is

$$\mathbf{u} = [F_x \ \delta_\mathrm{f} \ \delta_\mathrm{r}]^\mathrm{T}, \tag{13}$$

whereas the output vector of the plant is

$$\mathbf{q} = [u \ v \ r]^\mathrm{T}. \tag{14}$$

Equation (10) is rearranged in the following form:

$$\dot{\mathbf{q}} = (-\mathbf{M}^{-1}\mathbf{A}_1)\mathbf{q} + (-\mathbf{M}^{-1}\mathbf{B}_1)\mathbf{u} + (-\mathbf{M}^{-1}\mathbf{W}_1) = \mathbf{A}\mathbf{q} + \mathbf{B}\mathbf{u} + \mathbf{W}, \tag{15}$$

which will be used for robust control design.

2.3. *Conventional 2DOF linear model*

In this section, the 2DOF linear model, which has been extensively used by researchers for controller design, is presented for comparison. This model will be used for designing a state-feedback controller, which is also a common practice, for the purpose of performance comparison.

The 2DOF model is obtained by assuming that the vehicle's forward velocity u is constant. This eliminates the need to consider the first equation of motion in Equation (10). In addition, the term $\mathbf{W}_1$ is neglected in the literature. The 2DOF model is represented by

$$\mathbf{M}_{(2\mathrm{D})}\dot{\mathbf{q}}_{2\mathrm{D}} + \mathbf{A}_{1(2\mathrm{D})}\mathbf{q}_{2\mathrm{D}} + \mathbf{B}_{1(2\mathrm{D})}\mathbf{u}_{2\mathrm{D}} = \mathbf{0}, \tag{16}$$

where

$$\mathbf{M}_{(2\mathrm{D})} = \begin{bmatrix} m & 0 \\ 0 & I_z \end{bmatrix}, \quad \mathbf{A}_{1(2\mathrm{D})} = \begin{bmatrix} \dfrac{C_{\alpha\mathrm{f}} + C_{\alpha\mathrm{r}}}{u} & mu + \dfrac{C_{\alpha\mathrm{f}}a - C_{\alpha\mathrm{r}}b}{u} \\ \dfrac{C_{\alpha\mathrm{f}}a - C_{\alpha\mathrm{r}}b}{u} & \dfrac{C_{\alpha\mathrm{f}}a^2 + C_{\alpha\mathrm{r}}b^2}{u} \end{bmatrix},$$

$$\mathbf{B}_{1(2\mathrm{D})} = \begin{bmatrix} -C_{\alpha\mathrm{f}} & -C_{\alpha\mathrm{r}} \\ -aC_{\alpha\mathrm{f}} & bC_{\alpha\mathrm{r}} \end{bmatrix}. \tag{17}$$

The linear model in Equation (16) is used as the plant model. The input vector and the output vector are

$$\mathbf{u}_{2\mathrm{D}} = [\delta_\mathrm{f}, \delta_\mathrm{r}]^\mathrm{T}, \quad \mathbf{q}_{2\mathrm{D}} = [v, r]^\mathrm{T}, \tag{18}$$

respectively. Equation (16) is rearranged in the following form:

$$\dot{\mathbf{q}}_{2\mathrm{D}} = (-\mathbf{M}_{(2\mathrm{D})}^{-1}\mathbf{A}_{1(2\mathrm{D})})\mathbf{q}_{2\mathrm{D}} + (-\mathbf{M}_{(2\mathrm{D})}^{-1}\mathbf{B}_{1(2\mathrm{D})})\mathbf{u}_{2\mathrm{D}} = \mathbf{A}_{2\mathrm{D}}\mathbf{q}_{2\mathrm{D}} + \mathbf{B}_{2\mathrm{D}}\mathbf{u}_{2\mathrm{D}}, \tag{19}$$

which will be used for a state-feedback control design.

3. Control design

3.1. *Proposed nonlinear robust control for 3DOF model*

For the control design, a nominal model is defined based on the simplified 3DOF model presented in Equation (15). This nominal model has the following form:

$$\dot{\mathbf{q}} = \hat{\mathbf{A}}\mathbf{q} + \hat{\mathbf{B}}\mathbf{u}. \tag{20}$$

The desired trajectory of the system outputs are defined, in general, as a function of time:

$$\mathbf{q}^{\mathrm{d}}(t) = [u^{\mathrm{d}}(t)\ v^{\mathrm{d}}(t)\ r^{\mathrm{d}}(t)]^{\mathrm{T}}. \tag{21}$$

At any given time, the error of the outputs is defined as

$$\mathbf{e} = \mathbf{q} - \mathbf{q}^{\mathrm{d}}. \tag{22}$$

A first-order asymptotically stable desired error dynamics is defined and expressed as

$$\mathbf{s} = \mathbf{e} + \mathbf{\Lambda} \int_0^t \mathbf{e}\,\mathrm{d}t, \tag{23}$$

$$\dot{\mathbf{s}} = -\mathbf{K}\ \mathrm{sat}\left(\frac{\mathbf{s}}{\mathbf{\Phi}}\right), \tag{24}$$

where $\mathbf{\Lambda}$ is a positive-definite diagonal matrix, $\mathbf{K}$ is a diagonal gain matrix, and $\mathrm{sat}(\mathbf{s}/\mathbf{\Phi})$ is a column matrix whose elements are determined using the following relation.

$$\mathrm{sat}\left(\frac{s_i}{\phi_i}\right) = \begin{cases} \mathrm{sign}(s_i) & \text{if } |s_i| \geq \phi_i, \\ \dfrac{s_i}{\phi_i} & \text{if } |s_i| < \phi_i. \end{cases} \tag{25}$$

Normally, the introduction of a *constant* $\phi_i > 0$, called the 'boundary layer thickness', causes a smoother control input and *reduces* control input chattering.

Here, a *variable* ϕ_i is introduced to *eliminate* chattering altogether. Note that, for certain $\mathbf{K}$'s, Equation (24) drives the variable $\mathbf{s}$ to zero. When $\mathbf{s}$ is zero, the error $\mathbf{e}$ asymptotically approaches zero as dictated by Equation (23).

A control law that creates the desired error behaviour described by Equations (23) and (24) is derived by substituting Equation (23) in Equation (24), and using Equation (20) for $\dot{\mathbf{q}}$ in the result:

$$-\mathbf{K}\ \mathrm{sat}\left(\frac{\mathbf{s}}{\mathbf{\Phi}}\right) = \dot{\mathbf{e}} + \mathbf{\Lambda}\mathbf{e} = (\dot{\mathbf{q}} - \dot{\mathbf{q}}^{\mathrm{d}}) + \mathbf{\Lambda}\mathbf{e} = (\hat{\mathbf{A}}\mathbf{q} + \hat{\mathbf{B}}\mathbf{u} - \dot{\mathbf{q}}^{\mathrm{d}}) + \mathbf{\Lambda}\mathbf{e}. \tag{26}$$

The control law is obtained by solving Equation (26) for $\mathbf{u}$ as

$$\mathbf{u} = \hat{\mathbf{B}}^{-1}\left(\dot{\mathbf{q}}^{\mathrm{d}} - \mathbf{\Lambda}\mathbf{e} - \hat{\mathbf{A}}\mathbf{q} - \mathbf{K}\ \mathrm{sat}\left(\frac{\mathbf{s}}{\mathbf{\Phi}}\right)\right). \tag{27}$$

It can be seen that this control law is derived based on the nominal model of the vehicle represented by Equation (20). However, it must guarantee a good performance with Equation (15), which represents the actual model of the vehicle more closely. The parameter that can be determined to guarantee the good performance is the gain $\mathbf{K}$. In other words, the gain $\mathbf{K}$ must be

determined such that **e** tends to zero, despite a bounded difference between the control-oriented model (20) and the more accurate model (15). The bounded difference has two sources: first, neglecting nonlinear terms and second, uncertainty in the dynamic parameters used to evaluate $\hat{\mathbf{A}}$ and $\hat{\mathbf{B}}$.

The gain **K** is determined such that, for any initial condition for s_i in which $|s_i| > \phi_i$, $|s_i| \to \phi_i$ as $t \to \infty$, despite a bounded difference between the nominal and the more accurate model. This corresponds to the first condition presented in Equation (25), in which $\text{sat}(\mathbf{s}/\mathbf{\Phi}) = \text{sign}(\mathbf{s})$ (note that $\phi_i > 0$).[1] In other words, the gain **K** must be determined to make sure

$$\text{if } s_i \geq \phi_i > 0 \text{ (or } s_i - \phi_i \geq 0) \Longrightarrow \frac{\mathrm{d}}{\mathrm{d}t}(s_i - \phi_i) \leq -\eta_i \text{ (or } \dot{s}_i \leq \dot{\phi}_i - \eta_i), \tag{28}$$

$$\text{if } s_i \leq -\phi_i < 0 \text{ (or } -s_i - \phi_i \geq 0) \Longrightarrow \frac{\mathrm{d}}{\mathrm{d}t}(-s_i - \phi_i) \leq -\eta_i \text{ (or } -\dot{s}_i \leq \dot{\phi}_i - \eta_i), \tag{29}$$

where $\eta_i > 0$. Combining conditions in Equations (28) and (29) result in

$$s_i \dot{s}_i \leq |s_i|(\dot{\phi}_i - \eta_i), \tag{30}$$

or in the matrix form

$$\mathbf{s}^{\mathrm{T}} \dot{\mathbf{s}} \leq |\mathbf{s}|^{\mathrm{T}} (\dot{\mathbf{\Phi}} - \boldsymbol{\eta}). \tag{31}$$

Equation (31) represents the convergence condition.

The left-hand side of Equation (31) is expanded using the definition of **s** (Equation 23), the more accurate model (15), and the control law (27):

$$\begin{aligned} \mathbf{s}^{\mathrm{T}} \dot{\mathbf{s}} &= \mathbf{s}^{\mathrm{T}} (\dot{\mathbf{e}} + \mathbf{\Lambda e}) = \mathbf{s}^{\mathrm{T}} (\dot{\mathbf{q}} - \dot{\mathbf{q}}^{\mathrm{d}} + \mathbf{\Lambda e}) = \mathbf{s}^{\mathrm{T}} (\mathbf{A q} + \mathbf{B u} + \mathbf{W} - \dot{\mathbf{q}}^{\mathrm{d}} + \mathbf{\Lambda e}) \\ &= \mathbf{s}^{\mathrm{T}} (\mathbf{A q} + \mathbf{B}\hat{\mathbf{B}}^{-1} (\dot{\mathbf{q}}^{\mathrm{d}} - \mathbf{\Lambda e} - \hat{\mathbf{A}} \mathbf{q} - \mathbf{K}\, \text{sign}(\mathbf{s})) + \mathbf{W} - \dot{\mathbf{q}}^{\mathrm{d}} + \mathbf{\Lambda e}). \end{aligned} \tag{32}$$

Equation (32) is interesting in the sense that it includes the gain matrix **K** and terms form both the nominal and the more accurate model. Here, the bounds of difference between the two models can be exploited to determine **K** to satisfy Equation (31). It is assumed that the difference between $\hat{\mathbf{A}}$ and **A** is bounded:

$$|\mathbf{A} - \hat{\mathbf{A}}| \leq \tilde{\mathbf{A}}. \tag{33}$$

Furthermore, for a perfect nominal model with no parameter uncertainty, $\mathbf{B}\hat{\mathbf{B}}^{-1}$ would be the identity matrix. However, here this matrix is slightly different than the identity matrix. Its difference with the identity matrix is assumed to be bounded:

$$|\mathbf{B}\hat{\mathbf{B}}^{-1} - \mathbf{I}| \leq \tilde{\mathbf{B}}. \tag{34}$$

Finally, the matrix containing the neglected nonlinear terms, **W**, has a bound:

$$|\mathbf{W}| \leq \tilde{\mathbf{W}}. \tag{35}$$

Equation (32) is manipulated as

$$\begin{aligned} \mathbf{s}^{\mathrm{T}} \dot{\mathbf{s}} &= \mathbf{s}^{\mathrm{T}} ((\mathbf{A} - \hat{\mathbf{A}})\mathbf{q} + (\mathbf{B}\hat{\mathbf{B}}^{-1} - \mathbf{I})(\dot{\mathbf{q}}^{\mathrm{d}} - \mathbf{\Lambda e} - \hat{\mathbf{A}}\mathbf{q}) - \mathbf{B}\hat{\mathbf{B}}^{-1}\mathbf{K}\, \text{sign}(\mathbf{s}) + \mathbf{W}), \\ &\leq |\mathbf{s}^{\mathrm{T}}| (|\tilde{\mathbf{A}}\mathbf{q}| + \tilde{\mathbf{B}}|\dot{\mathbf{q}}^{\mathrm{d}} - \mathbf{\Lambda e} - \hat{\mathbf{A}}\mathbf{q}| - (\mathbf{I} + \tilde{\mathbf{B}}_{\mathrm{d}} - \tilde{\mathbf{B}}_{\mathrm{od}})\mathbf{K}_v + \tilde{\mathbf{W}}), \end{aligned} \tag{36}$$

where $\tilde{\mathbf{B}}_{\mathrm{d}}$ and $\tilde{\mathbf{B}}_{\mathrm{od}}$ are matrices consisting of only the diagonal and off-diagonal elements of $\tilde{\mathbf{B}}$, respectively. And $\mathbf{K}_v$ is a column matrix consisting the diagonal elements of the gain matrix

K. Now, comparing Equation (36) with the convergence condition (31) implies that $\mathbf{K}_v$ must be calculated as

$$\mathbf{K}_v(\mathbf{q}) = (\mathbf{I} + \tilde{\mathbf{B}}_{\mathrm{d}} - \tilde{\mathbf{B}}_{\mathrm{od}})^{-1}(|\tilde{\mathbf{A}}\mathbf{q}| + \tilde{\mathbf{B}}|\dot{\mathbf{q}}^{\mathrm{d}} - \boldsymbol{\Lambda}\mathbf{e} - \hat{\mathbf{A}}\mathbf{q}| + \tilde{\mathbf{W}} + \boldsymbol{\eta} - \dot{\boldsymbol{\Phi}}). \tag{37}$$

Using the values calculated from Equation (37) for the diagonal elements of the gain matrix **K** guarantees that if $|s_i| > \phi_i$, $|s_i| \to \phi_i$ as $t \to \infty$, which transitions $|s_i|$ into the second condition listed in Equation (25). In that situation, the **s** dynamics is

$$\dot{s}_i = -K_{vi}(\mathbf{q})\left(\frac{s_i}{\phi_i}\right) \quad |s_i| < \phi_i. \tag{38}$$

It is desirable that, inside the boundary layer, s_i asymptotically approaches zero with a constant rate of, say, $\lambda_{\phi i} > 0$, so that chattering is avoided. So, Equation (38) is rearranged as

$$\dot{s}_i + \left(\frac{K_{vi}(\mathbf{q})}{\phi_i}\right) s_i = 0, \quad \text{where } \frac{K_{vi}(\mathbf{q})}{\phi_i} = \lambda_{\phi i} > 0. \tag{39}$$

Since ϕ_i is small and $|s_i| \leq \phi_i$, s_i is small, which implies $\mathbf{q} \approx \mathbf{q}^{\mathrm{d}}$. So, Equation (39) is approximated as

$$\frac{K_{vi}(\mathbf{q}^{\mathrm{d}})}{\phi_i} = \lambda_{\phi i}, \tag{40}$$

or in the matrix form

$$\mathbf{K}_v(\mathbf{q}^{\mathrm{d}}) = \boldsymbol{\Lambda}_{\phi}\boldsymbol{\Phi}, \tag{41}$$

where $\boldsymbol{\Lambda}_{\phi}$ is a diagonal matrix with $\lambda_{\phi i}$'s as its diagonal elements. Now, the rate of change of $\boldsymbol{\Phi}$ that generates asymptotic convergence of **s** to zero is found by substituting Equation (37) in Equation (41):

$$\dot{\boldsymbol{\Phi}} = (|\tilde{\mathbf{A}}\mathbf{q}^{\mathrm{d}}| + \tilde{\mathbf{B}}|\dot{\mathbf{q}}^{\mathrm{d}} - \hat{\mathbf{A}}\mathbf{q}^{\mathrm{d}}| + \tilde{\mathbf{W}} + \boldsymbol{\eta}) - (\mathbf{I} + \tilde{\mathbf{B}}_{\mathrm{d}} - \tilde{\mathbf{B}}_{\mathrm{od}})\boldsymbol{\Lambda}_{\phi}\boldsymbol{\Phi}, \tag{42}$$

where the initial condition for $\boldsymbol{\Phi}$ is derived using Equation (41) at time zero. That is,

$$\boldsymbol{\Phi}(0) = \boldsymbol{\Lambda}_{\phi}^{-1}\mathbf{K}_v(\mathbf{q}^{\mathrm{d}}(0)). \tag{43}$$

In summary, the bounds of model mismatch are defined using Equations (33)–(35). Then, at each control step, $\dot{\boldsymbol{\Phi}}$ and $\boldsymbol{\Phi}$ are determined by using and integrating Equation (42) with initial condition (43). Finally, the elements of the gain matrix **K** are calculated from Equation (37), and the control action is derived using Equation (27), in which **s** is determined by Equation (23).

With this proposed controller, **e** vanishes as long as the bounds of the model mismatch are correctly estimated. In addition, the error behaviour inside the boundary layer, that is, $|s_i| < \phi_i$, is always smooth, so chattering is prevented at all times.

3.2. *Conventional linear control for the 2DOF model*

Here, for the purpose of comparison, a full-state feedback controller is designed using the 2DOF model (19). First, the error is defined as

$$\mathbf{e}_{2D} = \mathbf{q}_{2D} - \mathbf{q}^{d}_{2D}, \tag{44}$$

where $\mathbf{q}^{d}_{2D}$ represents the desired trajectory. The desired control input $\mathbf{u}^{d}_{2D}$ is found by substituting the desired trajectory in the dynamic model (19):

$$\dot{\mathbf{q}}^{d}_{2D} = \mathbf{A}_{2D}\mathbf{q}^{d}_{2D} + \mathbf{B}_{2D}\mathbf{u}^{d}_{2D}. \tag{45}$$

The error dynamics of the system is obtained by subtracting Equation (45) from Equation (19):

$$\dot{\mathbf{e}}_{2D} = \mathbf{A}_{2D}\mathbf{e}_{2D} + \mathbf{B}_{2D}(\mathbf{u}_{2D} - \mathbf{u}^{d}_{2D}). \tag{46}$$

A full-state feedback law is defined as

$$\mathbf{u}_{2D} = \mathbf{u}^{d}_{2D} - \mathbf{K}_{2D}\mathbf{e}_{2D}, \tag{47}$$

where $\mathbf{K}_{2D}$ is a diagonal gain matrix with k_{11} and k_{22} on the diagonal. Control law (47) generates the following closed-loop control behaviour:

$$\dot{\mathbf{e}}_{2D} = (\mathbf{A}_{2D} - \mathbf{B}_{2D}\mathbf{K}_{2D})\mathbf{e}_{2D}. \tag{48}$$

Several methods have been proposed for designing the gain matrix elements in the literature. Here, the pole placement method is used for simplicity. The characteristic polynomial of the closed-loop system (48) is calculated for the pole placement approach:

$$p^2 + c_1 p + c_2 = 0. \tag{49}$$

Assume that the closed-loop poles must be designed at $p = p_1$ and $p = p_2$. The desired characteristic equation that corresponds to these desired closed-loop poles is

$$p^2 - (p_1 + p_2)p + p_1 p_2 = 0, \tag{50}$$

which implies

$$c_1 = -(p_1 + p_2), \quad c_2 = p_1 p_2. \tag{51}$$

Equations (51) must be solved for the controller gains k_{11} and k_{22}, which are the diagonal elements of the gain matrix $\mathbf{K}_{2D}$. The gains k_{11} and k_{22} are calculated at each control time step to ensure that the closed-loop poles are constant while u changes.

4. Simulations and discussion

A 4WS vehicle is considered whose dynamic parameters are listed in Table 2.

The 3DOF robust controller has been designed to accommodate 20% parameter uncertainty in the dynamic model. That is, **A** and **B** in Equations (33) and (34) are estimated by using

parameters listed in Table 2 multiplied by 1.2. These parameters represent a small two-seater car (e.g. the unloaded mass of the Smart Roadster from Mercedes Benz (830 kg) plus a driver's mass and a small suitcase can bring up the mass to 917 kg). These estimates for $\mathbf{A}$ and $\mathbf{B}$ are used to determine $\tilde{\mathbf{A}}$ and $\tilde{\mathbf{B}}$. Also, the bound of the neglected nonlinear terms in the model, $\mathbf{W}$, is determined by assuming limits for control inputs as $F_{x\max} = 10,000\,\text{N}$, $\delta_{\text{f max}} = \pi/6\,\text{rad}$, $\delta_{\text{r max}} = \pi/6\,\text{rad}$.

The control parameters of the 3DOF nonlinear controller are $\mathbf{\Lambda} = \text{diag}_{3\times3}(10, 10, 10)$ and $\boldsymbol{\eta} = [15, 30, 15]^{\text{T}}$. The desired poles of the 2DOF conventional controller are $p_1 = -30$ and $p_2 = -30$.

For the simulations, the 3DOF nonlinear robust controller (Equation (27)) and the 2DOF conventional controller (Equation (47)) are applied to the 6DOF nonlinear dynamic model (Equation 1) with a full nonlinear Pacejka tire model (Equation (5)). The front (and rear) longitudinal force $F_{x\text{f}}$ (and $F_{x\text{r}}$) calculated by the controller is equally divided between the front (and rear) wheels of the 6DOF model. Also, the front (and rear) steering angles determined by the controller is used equally for both the front (and rear) wheels of the 6DOF model.

For the conventional controller, which is derived by assuming a constant u and neglecting the longitudinal dynamics, a simple proportional controller ($F_x = -3000(u - u^{\text{d}})$) is used to maintain the longitudinal speed. This mimics a driver's input to control the longitudinal speed.

In order to evaluate the robustness of the above controllers, two scenarios are considered for simulations. These scenarios are discussed below.

4.1. *Scenario 1: Turning with a variable speed*

The vehicle is initially travelling on a straight line with a speed of 1 m/s at time zero, when the driver decides to enter a turn with a constant radius of curvature of $\rho^{\text{d}} = 40\,\text{m}$ while increasing

Table 2. Simulation parameters.

$$\hat{m} = 917\,\text{kg}, \hat{I}_z = 1,128\,\text{kg m}^2, \hat{a} = 0.91\,\text{m}, \hat{b} = 1.64\,\text{m}, \hat{T} = 2.0\ \text{m},$$
$$\hat{C}_{\alpha\text{r}} = 57,296\,\text{N/rad}, \hat{C}_{\alpha\text{f}} = 52,712\,\text{N/rad}, \hat{\gamma} = 0.5, \hat{C}_{\text{D}} = 0.3, \hat{A}_{\text{D}} = 3.0\ \text{m}^2,$$
$$a_1 = -22.1, a_2 = 1011, a_3 = 1078, a_4 = 1.82,$$
$$a_5 = 0.208, a_6 = 0, a_7 = -0.354, a_8 = 0.707$$
$$A_{\text{f}} = 1.541, A_{\text{r}} = 2.857,$$
$$k_{1,2} = 289.3\,\text{kN/m}, k_{3,4} = 160.5\,\text{kN/m},$$
$$c_{1,2} = 32.6\,\text{kN s/m}, c_{3,4} = 24.3\,\text{kN s/m}$$

Note: $\hat{C}_{\alpha\text{f}}$ and $\hat{C}_{\alpha\text{r}}$ are found by fitting lines to the Pacejka model for $\alpha \in [-5°, 5°]$ (Figure 2).

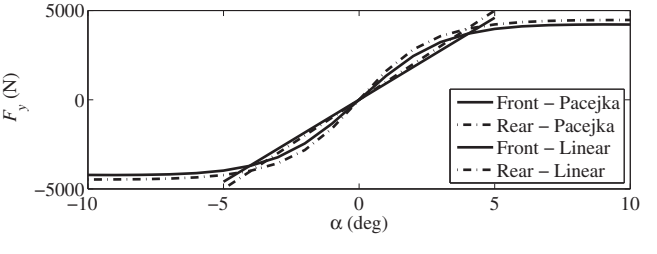

Figure 2. Finding estimates of tire stiffness for the 3DOF model using the Pacejka tire model.

the speed to 14 m/s in 20 s, after which the longitudinal speed remains constant at 14 m/s. The desired values for this scenario are defined as[2]

$$u^{\mathrm{d}}(t) = b_0 + b_1 t + b_2 t^2 + b_3 t^3 \text{ m/s}, \quad v^{\mathrm{d}} = 0 \text{ m/s}, \quad r^{\mathrm{d}} = \frac{u^{\mathrm{d}}}{\rho^{\mathrm{d}}} \text{ rad/s}, \tag{52}$$

where b_0, b_1, b_2, and b_4 are found such that the speed at time zero and time 20 s are 1 and 14 m/s, respectively, while the accelerations at times 0 and 20 s vanish. A wind gust with a negative longitudinal and a positive lateral component of approximately equal to 10% of the weight of the vehicle (917 N) is applied to the vehicle between the 8th and the 12th seconds of the simulated motion.

4.2. *Scenario 2: ISO TR 3888 lane change*

The standard ISO TR 3888 lane change manoeuvre is used to compare the performance of the two controllers. The nonlinear portions of the lane change manoeuvre are 7-order polynomials, whose slope and curvature have been used to define the desired yaw rate, while the desired longitudinal and lateral speeds are 18 m/s and zero, respectively.

4.3. *Discussion*

The paths of the vehicle for the two scenarios are shown in Figure 3. For scenario 1 (Figure 3(a)), it is seen that the path of the vehicle using the 3DOF nonlinear controller is still a perfect full circle with a constant radius. However, the vehicle under the 2DOF conventional control shows significant divergence from the circle just after the speed has slightly increased.

For scenario 2 (Figure 3(b)), it is seen that the path of the vehicle using the 3DOF nonlinear controller is a perfect lane change manoeuvre. However, the vehicle under the 2DOF conventional control shows significant divergence from the path. The tracking errors of the three speed components are shown in Figure 4. For scenario 1 (Figure 4(a)), the tracking error of the 2DOF controller increases with the increased speeds. However, the 3DOF is successful in keeping the tracking errors extremely close to zero. The same conclusion can be reached by studying Figure 4(b), which represents the speed errors for scenario 2. Figures 5(a) and (b) show the Euler angles of the 6DOF dynamic model used for simulations for the scenarios 1 and 2, respectively. It can be seen that, for both scenarios, the Euler angles caused by the 2DOF and the 3DOF controllers are very close to each other. However, the 2DOF controller results in roll and yaw angles that are higher than what they are needed to be for the exact manoeuvre. The control inputs for the two scenarios are shown in Figures 6(a) and (b). In

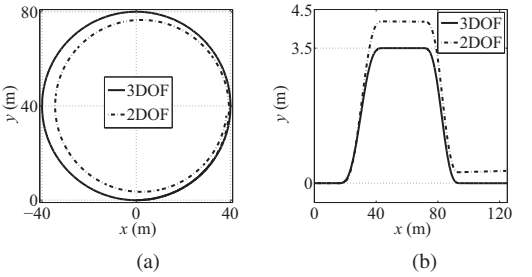

Figure 3. Vehicle's path. (a) Scenario 1. (b) Scenario 2.

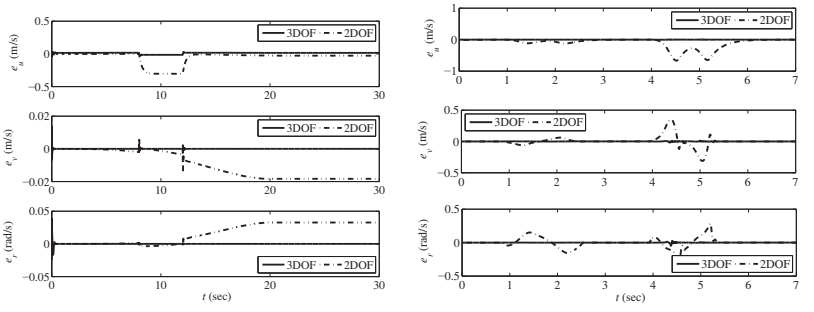

(a) (b)

Figure 4. Tracking errors. (a) Scenario 1. (b) Scenario 2.

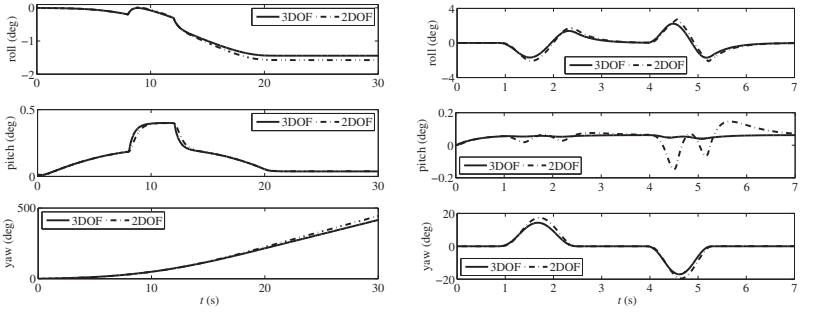

(a) (b)

Figure 5. Euler angles. (a) Scenario 1. (b) Scenario 2.

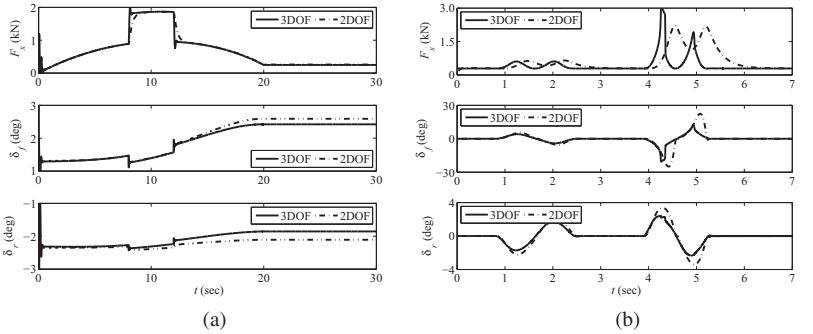

(a) (b)

Figure 6. Control inputs. (a) Scenario 1. (b) Scenario 2.

both scenarios, the 3DOF controller reacts much quicker to the disturbances than the 2DOF controller, and hence, it generates a much better performance. As a sample of the variable boundary behaviour, the surface variable s_1 for the longitudinal speed u and its corresponding variable boundary layer ϕ_1 are plotted in Figure 7. For this plot, which corresponds to scenario 1, an initial error in the longitudinal speed is assumed. It can be seen that the boundary layer grows rapidly to eliminate chattering at the beginning. Then, it automatically shrinks to provide better tracking accuracy. s_1 asymptotically approaches zero with no chattering.

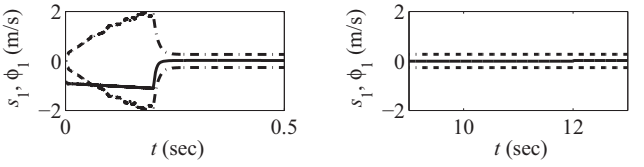

Figure 7. Variable boundary layer thickness for scenario 1. s_1 is the solid curve, and ϕ_1 is the dash-dot curve.

5. Conclusions

An approach is proposed for controlling the dynamics of 4WS vehicles, in which the longitudinal dynamics of the vehicle as well as its lateral and yaw motions are controlled simultaneously. With this approach, the effect of driving/braking forces of the tires on the lateral and yaw motions of the vehicle are included in the derived control laws. The control law is derived using the variable structure method, which is robust in the face of vehicle dynamic parameter uncertainty. A dynamically adaptive boundary layer is introduced to completely eliminate control chattering. The performance of the proposed controller is compared, via simulations, to that of a controller designed based on the conventional paradigm, in which the longitudinal speed is assumed to be constant, and only the lateral speed and the yaw rate dynamics are used for control law derivation. Simulations show that when parameter uncertainty and a variable longitudinal speed are introduced, it is best to use the proposed controller for excellent performance.

Notes

1. The second condition in Equation (25) will be discussed later.
2. Normally, front-wheel-steer vehicles are designed to be understeer. So, the lateral velocity of the centre of mass is non-zero due to the lateral slip. However, when designing a 4WS vehicle with drive-by-wire control, one has the option to 'tune' the controller to be understeer ($v^{\mathrm{d}} < 0$ for a right turn according to axes defined in Figure 1(b)), neutral steer ($v^{\mathrm{d}} = 0$), or oversteer ($v^{\mathrm{d}} > 0$ for a right turn). Here, as an example, for simplicity, the controller is tuned for neutral steer. Alternatively, choosing $v^{\mathrm{d}} = -u^{\mathrm{d}} \tan(5^\circ)\mathrm{sign}(r)$ mimics a constant 5° sideslip angle and gives the driver an understeer feel.

Nomenclature

$a_1, \ldots, a_8$	the parameters of the Pacejka tire model
A_{D}	frontal effective aerodynamic drag area
a	centre of mass distance to the front axle
b	centre of mass distance to the rear axle
C_{D}	frontal aerodynamic drag coefficient
c_i	damping of the shock absorber of the suspension at corner i
CM	centre of mass
$\mathbf{d}_i^{\mathrm{B}}$	position vector from the centre of mass to the ground contact point of tire i
$\mathbf{e}$	tracking error vector for 3DOF model (3×1)
$\mathbf{e}_{2\mathrm{D}}$	tracking error vector for 2DOF model (2×1)
e_u	tracking error of longitudinal speed

e_v	tracking error of lateral speed
e_r	tracking error of yaw rate
$\mathbf{F}_i^{\mathrm{B}}$	tire/ground reaction force vector
F_x	total driving force
F_{xi}	the longitudinal force for tire i
$F_{x\mathrm{f}}$	front axle driving force
$F_{x\mathrm{r}}$	rear axle driving force
F_{yi}	the lateral force for tire i
$F_{y\mathrm{f}}$	front axle lateral force
$F_{y\mathrm{r}}$	rear axle lateral force
F_{zi}	the vertical force for tire i
$\mathbf{g}^{\mathrm{B}}$	acceleration of gravity vector in vehicle body coordinates
$\mathbf{I}$	identity matrix (3×3)
$\mathbf{I}_G^{\mathrm{B}}$	mass moment of inertia matrix in vehicle body coordinates
I_z	vehicle yaw moment of inertia
$\mathbf{K}$	variable structure control diagonal gain matrix (3×3)
$\mathbf{K}_{2\mathrm{D}}$	state-feedback control diagonal gain matrix (2×2)
k_i	stiffness of the spring of the suspension at corner i
$\mathbf{K}_v$	vector containing diagonal elements of matrix $\mathbf{K}$ (3×1)
K_{vi}	elements of vector $\mathbf{K}_v$
k_{11}, k_{22}	diagonal elements of matrix $\mathbf{K}_{2\mathrm{D}}$
m	vehicle's mass
p	dummy parameter for closed-loop system's characteristic equation
p_1	desired pole 1 of the closed-loop system
p_2	desired pole 2 of the closed-loop system
$\mathbf{q}$	vector containing states of the 3DOF system (3×1)
$\mathbf{q}^{\mathrm{d}}(t)$	vector containing desired states of the 3DOF system (3×1)
$\mathbf{q}_{2\mathrm{D}}$	vector containing states of the 2DOF system (2×1)
$\mathbf{q}_{2\mathrm{D}}^{\mathrm{d}}$	vector containing desired states of the 2DOF system (2×1)
r	vehicle yaw rate
$\mathbf{r}_i^{\mathrm{B}}$	position vector from the centre of mass to the centre of tire i
$\mathbf{s}$	vector of surface parameters for variable structure controller (3×1)
$\mathrm{sat}(\cdot)$	saturation function operating on individual elements of vector $(\cdot)$
s_i	surface parameters for variable structure controller
$\mathrm{sign}(\cdot)$	sign function operating on individual elements of vector (.)
t	time
$\mathbf{u}$	vector of control inputs for the variable structure controller (3×1)
$\mathbf{u}_{2\mathrm{D}}$	vector of control inputs for the state-feedback controller (2×1)
u	vehicle longitudinal speed

v vehicle lateral speed

$\mathbf{V}_G^{\mathrm{B}}$ velocity vector of the centre of mass in vehicle body coordinates

z_i deflection in the spring of the suspension at corner i

δ_{f} average steering angle for front axle

δ_{r} average steering angle for rear axle

$\boldsymbol{\eta}$ minimum rate of convergence to surface for variable structure controller (3×1)

$\boldsymbol{\Phi}$ boundary layer thickness vector (3×1)

ϕ_i elements of vector $\boldsymbol{\Phi}$

γ front/rear driving force distribution ratio

$\boldsymbol{\Lambda}$ diagonal matrix for variable structure controller (3×3)

λ_i diagonal elements of matrix $\boldsymbol{\Lambda}$

$\boldsymbol{\omega}^{\mathrm{B}}$ angular velocity vector in vehicle body coordinates

ξ_{f} effective front axle average steering angle

ξ_{r} effective rear axle average steering angle

References

[1] G.-D. Yin, N. Chen, J.-X. Wang, and L.-Y. Wu, *A study on μ-synthesis control for four-wheel steering system to enhance vehicle lateral stability*, J. Dyn. Syst. Meas. Control Trans. ASME 133(1) (2011), pp. 2432–2439.

[2] M. Naraghi, A. Roshanbin, and A. Tavasoli, *Vehicle stability enhancement – an adaptive optimal approach to the distribution of tyre forces*, Proc. Inst. Mech. Eng. D: J. Automob. Eng. 224(4) (2010), pp. 443–453.

[3] B. Li and F. Yu, *Design of a vehicle lateral stability control system via a fuzzy logic control approach*, Proc. Inst. Mech. Eng. D: J. Automob. Eng. 224(3) (2010), pp. 313–326.

[4] G.-D. Yin, N. Chen, J.-X. Wang, and J.-S. Chen, *Robust control for 4WS vehicles considering a varying tire–road friction coefficient*, Int. J. Automot. Technol. 11(1) (2010), pp. 33–40

[5] J. Song and W.S. Che, *Comparison between braking and steering yaw moment controllers considering ABS control aspects*, Mechatronics 19(7) (2009), pp. 1126–1133.

[6] T. Hiraoka, O. Nishihara, and H. Kumamoto, *Automatic path-tracking controller of a four-wheel steering vehicle*, Veh. Syst. Dyn. 47(10) (2009), pp. 1205–1227.

[7] R. Marino and F. Cinili, *Input–output decoupling control by measurement feedback in four-wheel-steering vehicles*, IEEE Trans. Control Syst. Technol. 17(5) (2009), pp. 1163–1172.

[8] A. Alfi and M. Farrokhi, *Hybrid state-feedback sliding-mode controller using fuzzy logic for four-wheel-steering vehicles*, Veh. Syst. Dyn. 47(3) (2009), pp. 265–284.

[9] M. Canale and L. Fagiano, *Stability control of 4WS vehicles using robust IMC techniques*, Veh. Syst. Dyn. 46(11) (2008), pp. 991–1011.

[10] M. Chadli, A. Elhajjaji, and M. Oudghiri, *Robust output fuzzy control for vehicle lateral dynamic stability improvement*, Int. J. Model. Identification Control 3(3) (2008), pp. 247–257.

[11] G. Yin, N. Chen, and P. Li, *Improving handling stability performance of four-wheel steering vehicle via μ-synthesis robust control*, IEEE Trans. Veh. Technol. 56(5I) (2007), pp. 2432–2439.

[12] R. Marino, S. Scalzi, and F. Cinili, *Nonlinear PI front and rear steering control in four wheel steering vehicles*, Veh. Syst. Dyn. 45(12) (2007), pp. 1149–1168.

[13] H.-B. Yu and L. Gao, *Two-degree-of-freedom vehicle steering controllers design based on four-wheel-steering-by-wire*, Int. J. Veh. Auton. Syst. 5(1–2) (2007), pp. 47–78.

[14] A. El Hajjaji, A. Ciocan, and D. Hamad, *Four wheel steering control by fuzzy approach*, J. Intell. Robot. Syst. Theory Appl. 41(2–3) (2005), pp. 141–156.

[15] G. Zhengqi, L. Yufeng, and W. Seemann, *The performance of a vehicle with four-wheel steering control in crosswind*, Int. J. Veh. Auton. Syst. 1(2) (2003), pp. 256–269.

[16] H. Hu and Z. Wu, *Stability and Hopf bifurcation of four-wheel-steering vehicles involving driver's delay*, Nonlinear Dyn. 22(4) (2000), pp. 361–374.

[17] S. Horiuchi, K. Okada, and S. Nohtomi, *Effects of integrated control of active four wheel steering and individual wheel torque on vehicle handling and stability – a comparison of alternative control strategies*, Veh. Syst. Dyn. 33(1) (2000), pp. 680–691.

[18] M. Skarpetis and F. Koumboulis, *Multi-objective robust control for 4WS cars*, Syst. Control Theory Appl. (2000), pp. 169–171.

[19] A. Szosland, *Fuzzy logic approach to four-wheel steering of motor vehicle*, Int. J. Veh. Des. 24(4) (2000), pp. 350–359.
[20] S.-H. Lee, U.-K. Lee, S.-K. Ha, and C.-S. Han, *Four-wheel independent steering (4WIS) system for vehicle handling improvement by active rear toe control*, JSME Int. J. Ser. C: Dyn. Control Robot. Des. Manuf. 42(4) (1999), pp. 947–956.
[21] S.-S. You and Y.-H. Chai, *Multi-objective control synthesis: An application to 4WS passenger vehicles*, Mechatronics 9(4) (1999), pp. 363–390.
[22] J.-G. Song and Y.-S. Yoon, *Feedback control of four-wheel steering using time delay control*, Int. J. Veh. Des. 19(3) (1998), pp. 282–298.
[23] H.-F. Lin and A.A. Seireg, *Vehicle dynamics and stabilization using a nonlinear tyre model with four-wheel steering and braking*, Int. J. Comput. Appl. Technol. 11(1–2) (1998), pp. 53–64.